JCB Journal of Cell Biology

REPORT

Structural insights into G domain dimerization and pathogenic mutation of OPA1

Caiting Yu[1,2*], Jinghua Zhao[1,3*], Liming Yan[2*], Yuanbo Qi[1,3], Xiangyang Guo[1,3], Zhiyong Lou[2], Junjie Hu[1,3,4], and Zihe Rao[1,2,3]

The fusion of mammalian inner mitochondrial membranes (IMMs) is mediated by dynamin-like GTPase OPA1. Mutations in human OPA1 cause optic atrophy, but the molecular basis for membrane fusion and pathogenesis is not clear. Here, we determined the crystal structure of the minimal GTPase domain (MGD) of human OPA1. A three-helix bundle (HB) domain including two helices extending from the GTPase (G) domain and the last helix of OPA1 tightly associates with the G domain. In the presence of GDP and BeF_3^-, OPA1-MGD forms a dimer, the interface of which is critical for the maintenance of mitochondrial morphology. The catalytic core of OPA1 possesses unique features that are not present in other dynamin-like proteins. Biochemical experiments revealed that OPA1-MGD forms nucleotide-dependent dimers, which is important for membrane-stimulated GTP hydrolysis, and an N-terminal extension mediates nucleotide-independent dimerization that facilitates efficient membrane association. Our results suggest a multifaceted assembly of OPA1 and explain the effect of most OPA1 mutations on optic atrophy.

Introduction

Mitochondria are double membrane–bound organelles that frequently fuse and divide (Westermann, 2010). These membrane dynamics play important physiological roles, including mitochondrial genome maintenance (Belenguer and Pellegrini, 2013; Rodríguez-Nuevo et al., 2018; Vidoni et al., 2013). The fusion of mammalian inner mitochondrial membranes (IMMs) is mediated by dynamin-like GTPase OPA1 (Ban et al., 2017; Meeusen et al., 2006). Cells lacking OPA1 exhibit fragmented mitochondrial morphology and defects in cristae shaping (Del Dotto et al., 2017; Song et al., 2007). Deletion of OPA1 in mice is lethal (Davies et al., 2007; Zhang et al., 2011), and mutations in human OPA1 cause optic atrophy (Alexander et al., 2000; Delettre et al., 2000; MacVicar and Langer, 2016), but the underlying mechanism is not clear.

OPA1 and its yeast homologue Mgm1 belong to the dynamin superfamily. Similar dynamin-like proteins (DLPs) include atlastin (ATL), which mediates fusion of the ER (Hu and Rapoport, 2016), and mitofusin (MFN)/Fzo1, which mediates the fusion of outer mitochondrial membranes (Hoppins and Nunnari, 2009). Both ATL and MFN possess a classical N-terminal GTPase (G) domain followed by a helix bundle (HB) domain. Mechanistic studies of ATL and MFN have demonstrated that nucleotide-dependent dimerization of the G domain and movement of the HB domain relative to the G domain play critical roles in the fusion reaction. Recent structural studies of Mgm1 have revealed a similar configuration, in which the G domain is closely associated with an HB domain (Faelber et al., 2019; Yan et al., 2020). *Chaetomium thermophilum* Mgm1 has been visualized as a tetramer, similar to fission dynamins, the high-order assembly of which is proposed to remodel IMMs (Faelber et al., 2019). *Saccharomyces cerevisiae* Mgm1 (*Sc*Mgm1) forms a previously unidentified "head-to-tail" trimer that likely allows the fusion of IMMs (Yan et al., 2020). However, no G domain dimer has been observed in these structures.

Here, we determined the structure of a soluble module of human OPA1 and unveiled unique properties of nucleotide binding and hydrolysis by OPA1. Structural and biochemical analyses revealed that the G domain of OPA1 forms a nucleotide-dependent dimer, and a longer fragment with an N-terminal extension forms a dimer without nucleotide.

Results and discussion

Minimal G domain (MGD) construction is commonly used in the mechanistic investigation of dynamin and DLPs, including dynamin-1, a membrane fission protein, and mitofusin-1, the

[1]College of Life Sciences and State Key Laboratory of Medicinal Chemical Biology, Nankai University, Tianjin, China; [2]School of Medicine, Tsinghua University, Beijing, China; [3]National Laboratory of Macromolecules, Institute of Biophysics, Chinese Academy of Sciences, Beijing, China; [4]College of Life Sciences, University of Chinese Academy of Sciences, Beijing, China.

*C. Yu, J. Zhao, and L. Yan contributed equally to this paper; Correspondence to Junjie Hu: huj@ibp.ac.cn.

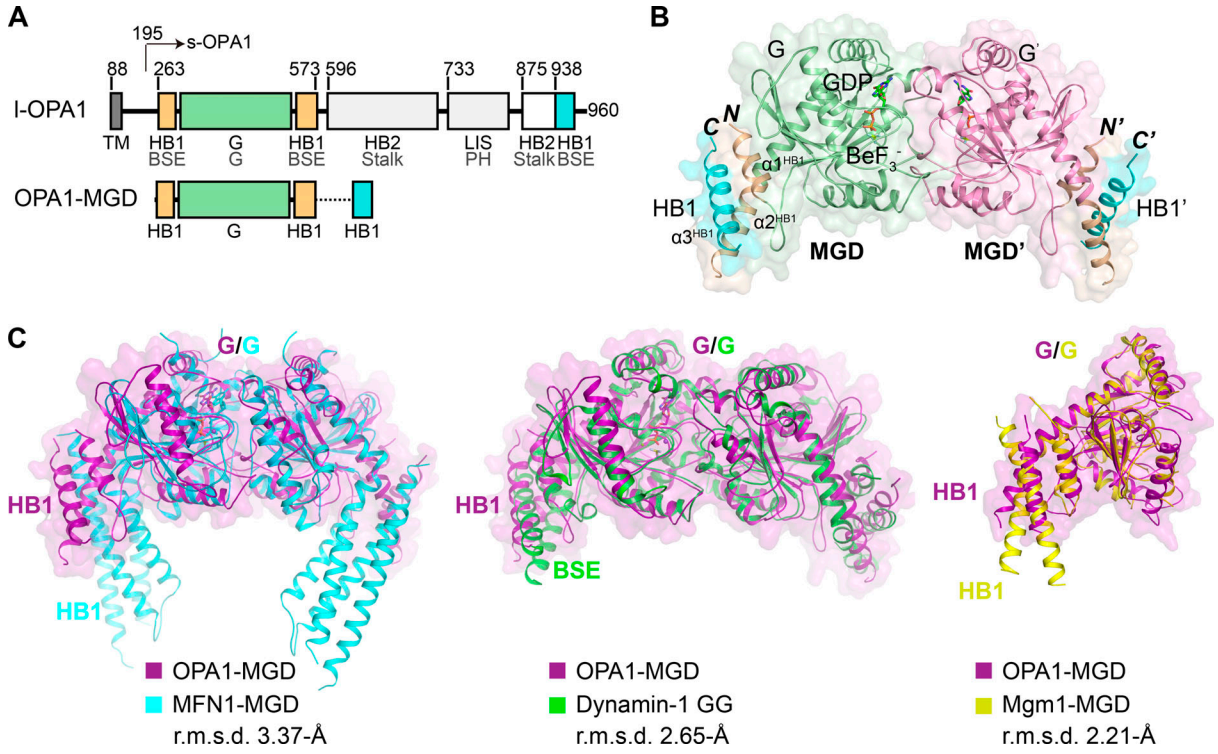

Figure 1. **Crystal structure of OPA1-MGD. (A)** Scheme showing the domains of human OPA1 and the MGD construct used for crystallization. Regions of OPA1 are colored and the residues numbered. Domains of OPA1 are labeled in black, with their corresponding domains in dynamin-1 in gray for comparison. HB1-forming helices that are connected to the GTPase are colored in yellow, the GTPase in green, and the C-terminal helices that complement HB1 and HB2 in cyan. TM, transmembrane domain; BSE, bundle signaling element; LIS, lipid-interacting stalk. **(B)** Structure of the GDP-BeF_3^--bound form of OPA1-MGD. Regions of OPA1 are colored as in A, except the G domain in the pairing molecule is colored purple. Termini are labeled in italics, and helices in the HB1 domain are numbered. Components in the pairing protomer are tagged with prime (′). A cartoon representation is shown with an overlaid surface view. **(C)** Superposition of OPA1-MGD with other DLPs. OPA1 is colored in magenta, MFN1 in cyan (PDB accession no. 5YEW), dynamin-1 in green (PDB accession no. 2X2F), and Mgm1 in yellow (PDB accession no. 6JSJ). Major domains are labeled. A surface representation of OPA1 is shown in all panels. The root mean squared deviation (r.m.s.d.) measurements are indicated.

fusogen for the outer mitochondrial membrane (Cao et al., 2017; Chappie et al., 2010; Jimah and Hinshaw, 2019; Qi et al., 2016; Yan et al., 2018). Full-length OPA1, also known as long form OPA1 (l-OPA1), is composed of an N-terminal transmembrane (TM) domain, a G domain, and a predicted long helical region (Fig. 1 A). Proteolysis in the linker between the TM and G domains releases short form OPA1 (s-OPA1, residues 195–960; Fig. 1 A; Del Dotto et al., 2018a; Ishihara et al., 2006; Olichon et al., 2007a). We combined N-terminal residues 263–580 with residues 938–960 at the C terminus using an artificial linker (GSGSGSGGS) to generate OPA1-MGD. The recombinant protein was expressed in *Escherichia coli*, purified, and crystallized in the presence of GDP and BeF_3^-. Given the potential similarity between OPA1-MGD and the equivalent dynamin-1 G domain construct, we determined the structure at 2.4-Å resolution by molecular replacement using the *Arabidopsis thaliana* dynamin-related protein 1A structure (PDB accession no. 3T35) as a search model (Table 1).

Two OPA1-MGD molecules were found in the asymmetric unit, and they formed a dimer with the two G domains facing one another (Fig. 1 B). As in other MGDs, a HB was attached to the G domain; it was formed by one helix preceding the G domain, one helix exiting the G domain, and the last helix from the C terminus of OPA1. The HB domain equivalent region in dynamin-1 is the bundle signaling element (BSE) domain (also termed GED for GTPase effector domain). Similar helical arrangements were seen in the dynamin-1 GTPase and GED (GG) dimer and the short form Mgm1 (s-Mgm1) structure. The orientation of the HB domain relative to the G domain resembles the transition state of dynamin-1 GG dimer, with the BSE adopting a semi-closed conformation (Chappie et al., 2010; Fig. 1 C); it is also virtually identical to the G and HB1 domains of s-Mgm1 in complex with GDP. The HB1 in MFN1-MGD is longer than that of Mgm1/OPA1 and dynamin-1. The HB1s of MFN1 in the closed state are closer to each other than those in the OPA1-MGD dimer. In addition, MFN1-HB1 consists of four helices instead of three. The extra helix comes from extension of the N terminus. When the sequences of Mgm1 and OPA1 were compared, a potential helix (residues 217–262, α0 of s-OPA1) was observed at the N terminus of the current OPA1 construct. When a peptide corresponding to residues 217–262 was synthesized and analyzed by circular dichroism (CD), a typical α-helix pattern was observed (Fig. 2 A). The inclusion of these residues renders extended OPA1-MGD (residues 217–580 and 938–960 connected by the artificial linker, termed 217-MGD) and s-OPA1 (residues 217–960, termed 217-s-OPA1) proteins

Table 1. **Data collection and refinement statistics**

Parameters (Data collection statistics)	**SeMet OPA1-MGD**
Data collection statistics	
Cell parameters	
a (Å)	77.9
b (Å)	77.9
c (Å)	171.5
α, β, γ (°)	90.0, 90.0, 90.0
Space group	*P43212*
Wavelength used (Å)	0.9798
Resolution (Å)	50.0–2.40 (2.49-2.40)[c]
No. of all reflections	472,513 (19,636)
No. of unique reflections	21,509 (2,067)
Completeness (%)	99.9 (98.9)
Average I/σ(I)	20.56 (1.52)
Rmerge[a] (%)	14.4(98.1)
Refinement statistics	
No. of reflections used (σ(F) > 0)	19,817
Rwork[b] (%)	21.2
Rfree[b] (%)	25.9
r.m.s.d. bond distance (Å)	0.01
r.m.s.d. bond angle (°)	1.408
Average B-value (Å2)	34.7
No. of protein atoms	2,559
No. of ligand atoms	35
No. of solvent atoms	143
Ramachandran plot	
res. in favored regions (%)	94.5
res. in allowed regions (%)	5.4
res. in outlier regions (%)	0.1

[a]Rmerge = ΣhΣl | Iih-Ih |/ΣhΣIIh where Ih is the mean of observations Iih of reflection h.
[b]Rwork = Σ(||Fp(obs)|-|Fp(calc)||)/Σ|Fp(obs)|. Rfree is an R factor for a pre-selected subset (5%) of reflections that was excluded in the refinement.
[c]Numbers in parentheses are corresponding values for the highest resolution shell.

(Fig. 2 B) without significant changes in their GTPase activity (Fig. 2, C and D). These results suggest that the OPA1-HB1/BSE domain may be a 4-HB. Notably, the N terminus of s-OPA1 (residues 195–216) is predicted to be a flexible region, suggesting that 217-s-OPA1 could closely represent features of the full-length s-OPA1.

GDP and BeF_3^- are well ordered in the nucleotide pocket of OPA1 (Fig. 3 A). In addition to the typical Mg^{2+} ion, a K^+ ion is present near the nucleotide. Similar organization has been reported for dynamin-1, but with a Na^+ ion instead, and MFN1 (Fig. 3, C and D), but this organization is not seen with Drp1, Mx, GBP, and ATL, suggesting a distinction in nucleotide processing between these DLPs. The Mg^{2+} ion in OPA1 is coordinated by T302 in G1/P-loop, T323 in G2/Switch 1, D398 in G3/Switch 2, the BeF_3^- moiety, and β-phosphate. The K^+ ion is engaged by S298 in the P-loop, the backbone oxygen of G317, E320 of Switch 1, the BeF_3^- moiety, and α- and β-phosphate (Fig. 3 B, right panel). Like in the dynamin-1 GG dimer structure (Chappie et al., 2010), a catalytic water molecule is placed near the BeF_3^- moiety by the backbone oxygen of T323 and the nitrogen of G401 in G3/Switch 2, and a bridging water molecule helps position the catalytic one by linking Q297 in G1/P-loop and the G401 carbonyl oxygen (Fig. 3 D and Fig. S1 D, left panel). In addition to what has been observed with dynamin-1 and MFN1, OPA1 possesses unique features in nucleotide interactions, particularly in Switch 1: (1) the guanine of GDP is stabilized with the help of T503 in the β6-α5 loop and R316 in Switch 1, as well as the canonical D470 and K468 in G4 (Fig. 3 B, left panel); (2) the winding Switch 1 is curved by the salt bridge of E320 and R324; and (3) it positions M321 and M322 for gating the nucleotide

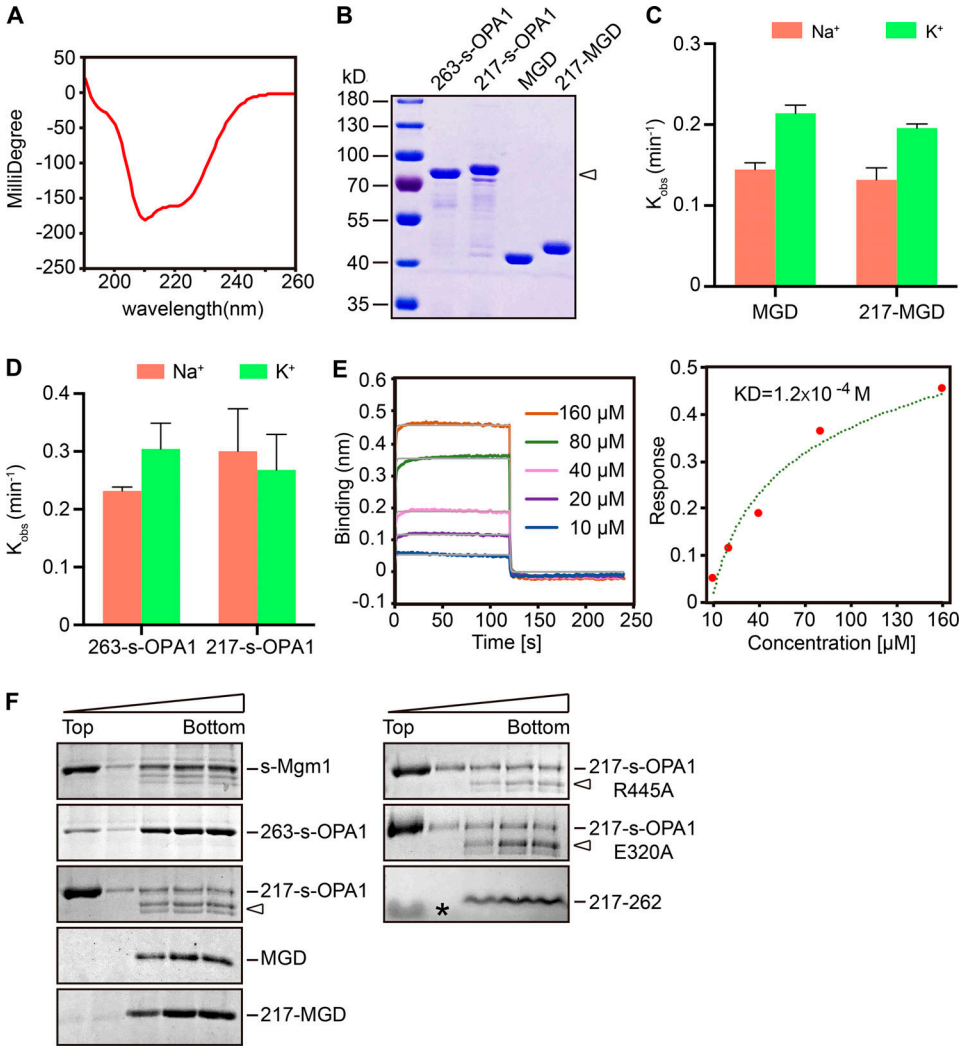

Figure 2. **N-terminal coiled coil and lipid interactions of OPA1. (A)** CD spectrum of the 217–262 peptide at 60 µM. Negative peaks at 208 nm and 222 nm indicate a typical α-helix. **(B)** Purified 263-s-OPA1, MGD, 217-s-OPA1, and 217-MGD (N-terminal extended version, starts from residue 217) were analyzed by SDS-PAGE and Coomassie blue staining. Degradation products of 217-s-OPA1 are indicated by an arrowhead. **(C)** The GTPase activity of the indicated OPA1-MGD proteins was measured in the presence of 250 mM NaCl or KCl and 4 mM $MgCl_2$. 10 µM of protein was used for each sample. GTP hydrolysis was measured by phosphate release at saturating GTP concentrations (1 mM). The rate constant Kobs was shown as µM Pi release per minute per µM protein. Data are presented as the mean ± SD of three measurements and representative of at least three repetitions. **(D)** As in C, but with the indicated s-OPA1. **(E)** BLI analysis of self-association of the 217–262 peptide. Biotinylated peptides were immobilized to streptavidin sensors. A gradient concentration of 10–160 µM of unlabeled peptides was used. Response curve of the steady-state fit provides a dissociation constant (K_D). Data are representative of three biological repeats. **(F)** Liposome flotation assay with various OPA1 constructs. Liposomes (2 mM, POPC/POPE/CL/PI/Rhodamine-PE = 47:23.5:20:8:1.5) were mixed with 2 µM purified protein or 10 µM peptide at room temperature for 30 min. Fractions collected after centrifugation were analyzed by SDS-PAGE and Coomassie blue staining. The data are representative of at least three repetitions. Degradation products of 217-s-OPA1 are indicated by arrowheads. A lipid band is indicated by an asterisk (*).

pocket. These features are only partially conserved in Mgm1 (Fig. 3 C).

To test the nucleotide binding by OPA1, we performed isothermal titration calorimetry (ITC). OPA1-MGD binds to GDP at a dissociation constant (K_D) of 5.5 µM (Fig. 3 E, left panel) in K^+-containing buffer. Unexpected lower affinities were detected with nonhydrolysable GTP analogue GTPγS (10.0 µM; Fig. 3 E, right panel), likely because of subtle differences between GTP and GTPγS. Further lower affinities were measured when the ITC was performed in Na^+-containing buffer (13.4 µM and 18.9 µM; Table S1). When GMPPNP, a different nonhydrolysable GTP analogue, was used with K^+- or Na^+-containing buffer, less interaction was observed (Fig. S1 A), again suggesting that GMPPNP is less fitted in the nucleotide pocket due to subtle chemical variation. Similarly, no interaction was detected with GMPPCP (Fig. S1 A). Overall, the nucleotide interactions with OPA1 were similar to *C. thermophilum* Mgm1 (K_D = 9 µM to GTPγS), stronger than the nucleotide interactions with *Sc*Mgm1 and MFN1 (K_D = 30–90 µM), and weaker than the nucleotide interactions with ATL1 (K_D = 1–2 µM), the fusogenic DLP in the ER. Notably, OPA1 exhibited relatively high affinity for GDP among mitochondrial

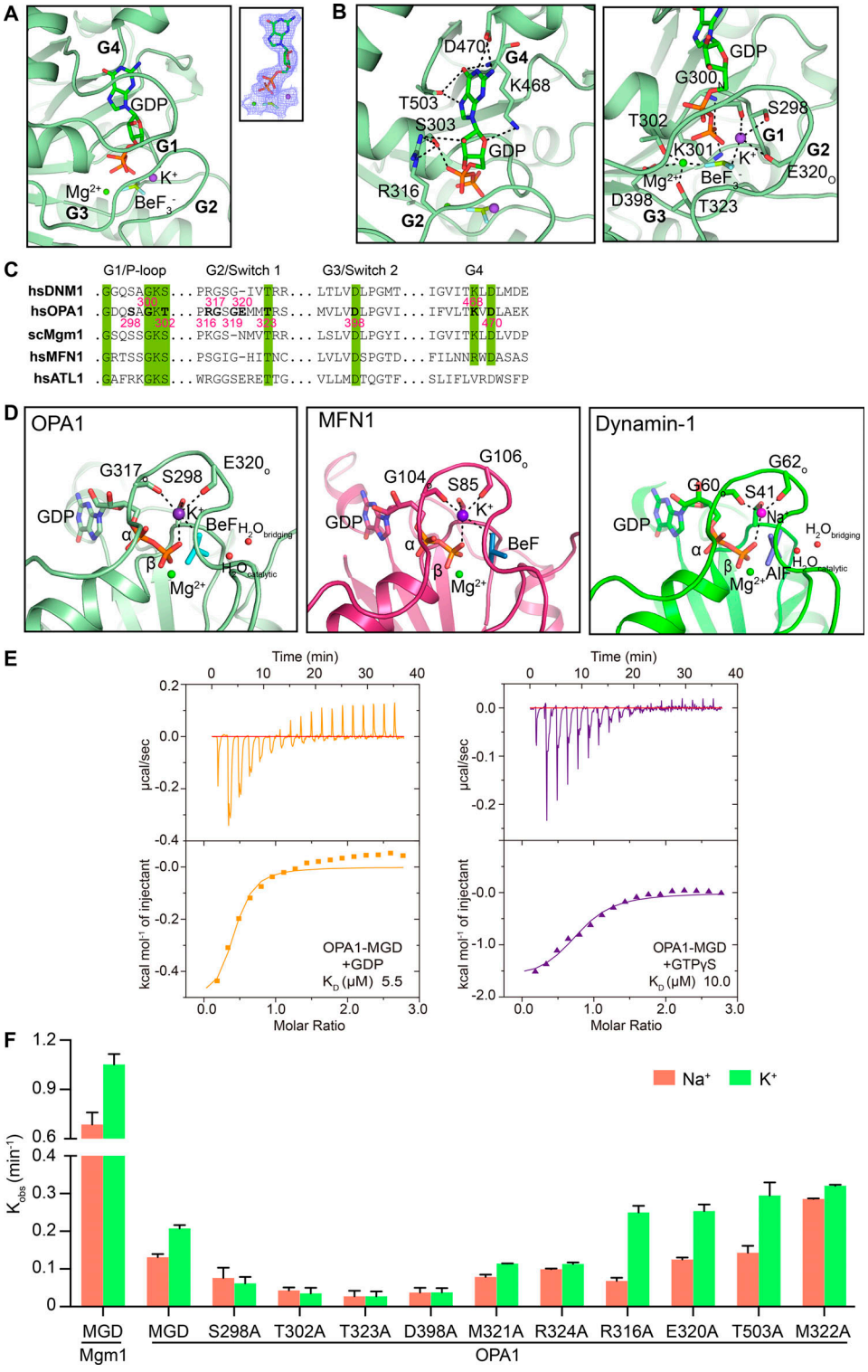

Figure 3. **Nucleotide binding and GTP hydrolysis of OPA1. (A)** GDP-BeF_3^- in the active site of OPA1 is shown in stick form. The 2Fo - Fc electron density maps (1.0σ contour) of GDP are shown as wire mesh (blue). **(B)** Interactions in the catalytic core. **(C)** Sequence alignment of the signature motifs of OPA1 and similar DLPs. **(D)** Comparison of the active sites of OPA1, MFN1 (PDB accession no. 5YEW), and dynamin-1 (PDB accession no. 2X2F). **(E)** Binding affinity of GDP and GTPγS for OPA1-MGD was measured by ITC in the buffer containing 150 mM KCl. A 2 mM nucleotide solution was titrated stepwise into 0.15 mM protein. The dissociation constant (K_D) is given in the inset. The data are representative of at least three repetitions. **(F)** The GTPase activity of various OPA1 constructs was measured in the presence of 250 mM NaCl or KCl and 4 mM $MgCl_2$. For Mgm1, the measurement was performed in buffer containing 500 mM NaCl or KCl and 5 mM $MgCl_2$. 10 µM of protein was used for each sample. GTP hydrolysis was measured by phosphate release at saturating GTP concentrations (1 mM). Data are presented as the mean ± SD of three measurements and representative of at least three repetitions.

fusion DLPs, suggesting a slower release of GDP and a delayed reset of a new hydrolysis cycle.

When K^+ was included in the buffer, the GTPase activity of OPA1-MGD was approximately twofold higher than with Na^+, possibly because K^+ is more efficient than Na^+ in organizing the vicinity of the nucleotide for GTP hydrolysis. The preference of OPA1 for K^+ during GTP hydrolysis, which is consistent with a much higher intracellular concentration of K^+ than that of Na^+, is reproducible and more evident when protein concentrations are high (Fig. S1 B), but not as strong as with human MFN1 (approximately fivefold higher with K^+ than with Na^+; Yan et al., 2018). Removal of the N-terminal His tag did not affect the GTPase activity (Fig. S1 C). Interestingly, the GTPase activity of OPA1 is two- to threefold lower than that of *Sc*Mgm1 (Fig. 3 F), despite their similarity in G domain signature motifs (Fig. 3 C). One possible explanation is that OPA1 holds onto GDP longer than Mgm1, as mentioned above, therefore delaying the recycle.

Next, we performed ITC by mutating residues in the nucleotide pocket, all in K^+-containing buffer. The results were in general consistent with structural prediction. S298 coordinated the K^+ ion but did not directly contact the nucleotide. S298A exhibited no significant defects in GTPγS interactions but a decreased affinity for GDP (Table S1). T302 (equivalent to S45 in dynamin-1), which likely stabilizes the Mg^{2+} in both GDP- and GTP-bound states, had drastically reduced interactions with both GDP and GTPγS, whereas the highly conserved T323 (equivalent to T65 in dynamin-1) and D398 had two- to threefold decreases (Table S1). M322 of Switch 1, which is much closer to the catalytic core than the neighboring M321 and shields the K^+ ion and the nucleotide, drastically affected binding to GTPγS and GDP when mutated to Ala, whereas M321A had a weaker impact (Table S1). We also tested the guanosine-interacting residues that are unique to OPA1. Surprisingly, T503A had largely unchanged affinity for GDP or GTPγS (Table S1), possibly adopting the change by using main chain atoms instead. In contrast, R316A decreased interactions with GTPγS, but not GDP (Table S1), suggesting a possible adaptation only in the GDP-bound state. Finally, R324A, which is predicted to compromise the bending of Switch 1, had greatly reduced affinity for both GDP and GTPγS (Table S1).

When highly conserved residues in G motifs, including S298, T302, T323, and D398, were mutated to Ala in OPA1-MGD, the GTPase activity was drastically reduced in both Na^+- and K^+-containing buffers (Fig. 3 F). Interestingly, the two hydrophobic residues in Switch 1, M321 and M322, had opposite effects on GTP hydrolysis, with a decrease for M321A and increase for M322A (Fig. 3 F), but both lacked a preference for cation type (K^+ vs. Na^+). It is possible that substitution of M322, which affected nucleotide binding, could be compensated by an unknown rearrangement of the Switch 1. Consistent with nucleotide-interacting ability, R316A, but not T503A, had altered GTPase activity (Fig. 3 F). Notably, R316A had half the WT activity in Na^+ but slightly increased activity to WT in K^+, suggesting a lack of dependence on R316-mediated guanine interaction under physiological conditions. Finally, R324A had equivalent activity to WT in Na^+ but only half the activity of WT in K^+ (Fig. 3 F), confirming the key role of Switch 1 bending in cooperation with K^+. These results underscore the plasticity of Switch 1 upon mutagenesis and suggest that GTP hydrolysis by OPA1 is precisely regulated by coordinated G motifs, particularly Switch 1, using mechanisms in addition to the previously identified one with other DLPs.

The OPA1-MGD dimer interface buries a surface area of 1,573.3 $Å^2$ (Fig. S2 A) with a K_D of 2.9 μM (Fig. S2 B), stronger than dynamin-1 GG dimer (Chappie et al., 2011; ∼8.4 μM in the presence of GDP and AlF_4^-). The dimer is generated by two sets of symmetric interactions. First, R445 in the β4-α3 loop forms a salt bridge with D438 in the same loop of the pairing molecule (Fig. 4 A, box 1). Notably, D438 is stabilized by K468 in G4. The β4-α3 loop in dynamin-1 was previously termed the "trans stabilizing loop" for dimerization of the MGD. S298 in G1/P-loop hydrogen bonds with D442 in the β4-α3 loop of the other protomer. Second, E320 in G2/Switch 1 reaches S478 in the other molecule, and the backbone oxygen of G319 forms hydrogen bonds with R481 (Fig. 4 A, box 2). Notably, G319 is not only involved in dimer formation, but also plays a role in K^+ coordination through S298, and this residue is missing in G2/Switch 1 of Mgm1 (Fig. S1 D, right panels). In addition, T407 in G3/Switch 2 pairs with E444 in the β4-α3 loop. The position of T407 is partly ensured by intramolecular hydrogen bonding between T376 of the β2-connecting loop and T414/A411 near G3/Switch 2. Notably, the β2-connecting loop corresponds to the "cis stabilizing loop" in the dynamin-1 GG dimer. Collectively, dimerization of OPA1-MGD is realized by unprecedented intertwining of the two stabilizing loops and elements from all four signature G motifs. These observations predict that GTP hydrolysis by OPA1, possibly assembly-stimulated hydrolysis, could be linked to dimer formation.

Next, we measured nucleotide-dependent dimerization by analytical gel filtration combined with multi-angle light scattering (MALS). OPA1-MGD dimerized in the presence of GDP and BeF_3^- in a K^+-dependent manner (Fig. 4 B). Nearly two thirds of OPA1-MGD molecules were dimers when incubated with K^+ and gel filtered with K^+-containing buffer. Dimer was not found without nucleotide or with GDP or GTPγS (Fig. S2 C). Strikingly, dimers were not formed when the protein was preincubated with GDP and BeF_3^- in K^+-containing buffer and subsequently run in Na^+-containing buffer, or vice versa, for MALS analysis (Fig. S2 D). The same results were obtained with analytical ultra-centrifugation (AUC); dimers only formed with GDP and BeF_3^- in K^+-containing buffer (Fig. 4 C). As expected, substitution of R445 with Ala significantly abolished dimer formation in MALS tests (Fig. 4 B). Similar results were obtained with other mutants of the dimer interface, including E320A, T407A, D442A, and E444A (Fig. 4 B). Interestingly, when dimer formation was analyzed by AUC, all except E320A had the same consistent results. The discrepancy is likely caused by different stringency of the tests, as loaded protein would be diluted during MALS. Furthermore, we measured nucleotide binding and GTP hydrolysis and found very minor defects in these mutants (Fig. 3 F, Table S1, and Fig. S1 E). These results suggest that residues identified at the dimer interface regulate nucleotide-dependent dimerization, with E320A to a lesser extent.

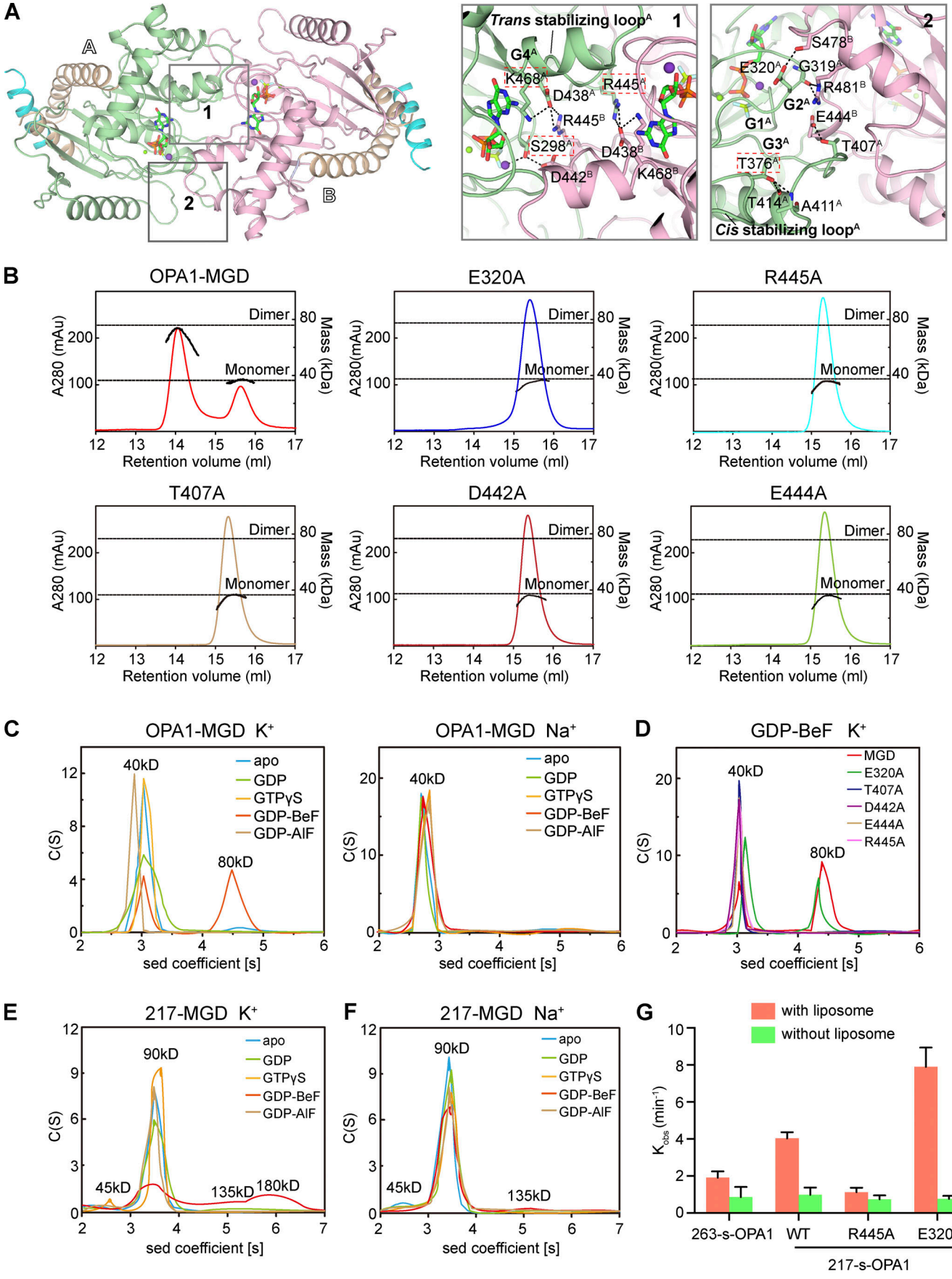

Figure 4. **Dimerization of OPA1. (A)** Dimer interface of OPA1-MGD. Key regions are boxed, and a stick representation of key residues is shown. The two protomers are labeled as A and B. **(B)** The sizes of WT OPA1-MGD and mutants (theoretical molecular mass 39 kD) were determined by MALS coupled with gel filtration in the presence of 0.5 mM GDP and 2.5 mM BeF_3^- with running buffer containing 150 mM KCl and 4 mM $MgCl_2$. The estimated molecular masses are shown on the right axis. mAu, milli-Absorbance Unit. The data are representative of at least three repetitions. **(C)** The size of OPA1-MGD was determined at 25 µM by AUC in the absence or presence of the indicated nucleotides in a buffer containing 150 mM KCl or NaCl. The estimated molecular masses are given above the peaks (in kilodaltons). Sed, sedimentation. The data are representative of at least three repetitions. **(D)** As in C, but with the indicated mutants of OPA1-MGD (theoretical molecular mass, 39 kD) in the presence of 0.5 mM GDP and 2.5 mM BeF_3^- in running buffer containing 150 mM KCl and 4 mM $MgCl_2$. The data are representative of at least three repetitions. **(E)** As in C, but with 217-MGD (theoretical molecular mass 44.6 kD). The data are representative of at least three repetitions. **(F)** As in E, but in Na^+-containing buffer. **(G)** The GTPase activity of the indicated OPA1 proteins was measured in the absence or presence of 0.2 mM IMM mimicking liposomes (47:23.5:20:8:1.5 mol % POPC/POPE/cardiolipin/soy-PI/Rhodamine-PE). 2 µM protein was incubated and 1 µM used for measurements. GTP hydrolysis was measured by phosphate release at saturating GTP concentrations (1 mM). Data are presented as the mean ± SD of three measurements and representative of at least three repetitions.

In the process of purifying 217-MGD, we noticed that the protein was eluted at a higher molecular weight than MGD, suggesting that the region of 217 to 262 may mediate homotypic interactions. Therefore, we performed biolayer interferometry (BLI) using synthesized peptides in this region. Biotinylated 217–262 peptide was immobilized to the streptavidin sensor surface and incubated with increasing concentrations (10–160 µM) of unmodified peptide. The association and disassociation between peptides, which influenced the thickness of the layer on the sensor tip, was monitored as an interference wavelength shift. The self-association affinity of the peptide was determined to be ∼0.12 mM, weak but detectable (Fig. 2 E). Consistently, AUC analysis revealed that 217-MGD formed dimer without nucleotide (Fig. 4 E), even in Na^+-containing buffer (Fig. 4 F). The addition of various nucleotides did not alter the dimerization tendency (Fig. 4, E and F). These results suggest that OPA1 may dimerize independent of nucleotide using its N-terminal region, likely acting in a coiled-coil manner. In addition, this helix is less likely to complement the HB1 domain than initially predicted.

Membrane-associated assembly of DLPs, including OPA1, has been reported to stimulate GTP hydrolysis. We first tested whether various OPA1 constructs interact with membranes in a flotation assay. Purified OPA1 fragments were incubated with IMM-mimicking liposomes (47% 1-palmitoyl-2-oleoyl-sn-glycero-3-phosphocholine, 23.5% 1-palmitoyl-2-oleoyl-sn-glycero-3-phosphoethanolamine, 20% cardiolipin, 8% soy phosphatidylinositol, and 1.5% Rhodamine-phosphoethanolamine) and placed in the bottom of a sucrose-density gradient. Centrifugation resulted in flotation of liposomes to the top fractions, and co-flotation of proteins with these fractions indicated an association. Truncated s-OPA1 containing residues 263–960 had a weak interaction, but 217-s-OPA1, which is close to the full-length OPA1, exhibited efficient lipid association (Fig. 2 F). An s-Mgm1 construct (residues 184–881) equivalent to 217-s-OPA1 interacted similar to 217-s-OPA1 in the same conditions (Fig. 2 F). We reported recently that the MGD of Mgm1 possesses lipid-interacting sites in addition to the conventional sites in the C terminus. Therefore, we tested whether OPA1-MGD also binds to membranes. 217-MGD exhibited a very weak but reproducible association with IMM liposomes, whereas the shorter version had no detectable association (Fig. 2 F). The difference in lipid interaction between the 217 version and 263 version suggests that either the 217–262 region contains additional lipid-binding sites, or the dimerization that occurs here increases local concentrations of lipid-approaching OPA1. The lack of flotation by the 217–262 peptide supported the latter possibility (Fig. 2 F). Taken together, the results indicate that s-OPA1 likely engages IMMs in an Mgm1-like manner.

Next, we measured membrane-stimulated GTP hydrolysis of OPA1 (Fig. 4 G). 263-s-OPA1 exhibited a mild twofold stimulation. Further stimulation was detected when 217-s-OPA1, which has enhanced nucleotide-independent dimerization, was used. As expected, the R445A mutant, which disrupts the nucleotide-dependent G domain dimer, abolished the stimulated GTP hydrolysis of 217-s-OPA1. Interestingly, E320A, a very weak mutant at the dimer site, exhibited an increase in membrane-stimulated GTP hydrolysis. Notably, the membrane interaction was not altered with these two mutants (Fig. 2 F). Collectively, these results confirm that OPA1 is capable of stimulating GTPase activity upon lipid association, and both nucleotide-dependent and -independent dimerization play important roles.

Most of the published OPA1 mutations causing optic atrophy (Ban et al., 2010; Carelli et al., 2015; Del Dotto et al., 2018b; Kircher et al., 2014) are localized in the MGD region (Fig. 5 A). The modeled mutations can be categorized into four types: (1) S298N (G1 motif), G300E, K468E (G4 motif), and K505N involved in nucleotide binding (Fig. 5 A, box 1); (2) S298N, T376A, G439V, R445H, T449P, and K505N affecting dimer formation (Fig. 5 A, box 2); (3) R290Q, I313K, I382M, and L384F regulating the folding of the G domain core (Fig. 5 A, box 3); and (4) D273A, S545R, R571H, and L939P, which ensure packing of HB1 and may have other functions that are yet to be identified (Fig. 5 A, box 4). We tested several disease mutations in OPA1-MGD dimerization. As expected, G300E lost the nucleotide interaction. S298A, R445H, and L939P all demonstrated normal affinity with GTPγS but reduced affinity with GDP (Table S1). MALS analysis revealed that S298A, G300E, and R445H nearly abolished dimer formation and I328M and L939P significantly reduced it (Fig. 5 C). Similar changes were observed with AUC analysis (Fig. 5 D). Importantly, all mutants, except the nucleotide-interacting incompetent G300E, had normal to slightly increased GTPase activity, suggesting that intact basal GTPase activity of OPA1 could not simply translate into normal protein function.

We were also able to deduce the roles of mutations in the remaining parts of s-OPA1 based on sequence comparisons and the structural information from s-Mgm1 (Fig. 5 B). s-Mgm1 folds into a dynamin-1–like conformation. In addition to the MGD, s-Mgm1 has an HB2 domain (equivalent to the stalk domain of

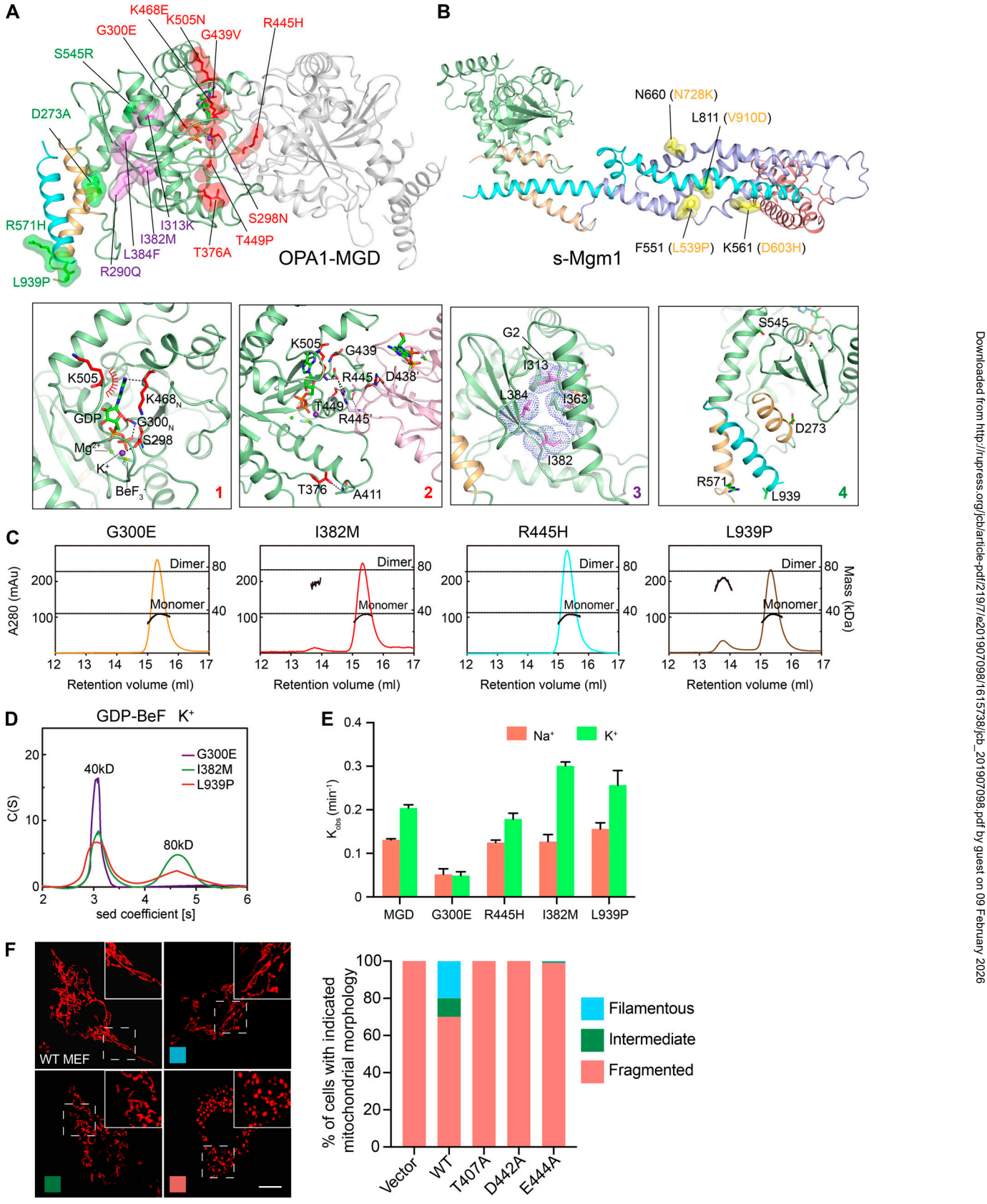

Figure 5. **Disease-causing mutations in OPA1. (A)** Cartoon representation of the OPA1-MGD dimer. Disease-causing mutations are shown in stick form with a spherical surface. Mutations that are related to nucleotide binding and/or dimerization are colored in red. Mutations that affect folding of the G domain are colored in purple. Other mutations are colored in green. Interactions with the mutated residues are shown in boxes with zoomed-in views. **(B)** As in A, but with

OPA1 mutations that are outside the MGD and can be mapped onto the s-Mgm1 structure. These residues are shown in stick form with a spherical surface and colored in yellow. **(C)** The sizes of OPA1-MGD mutants (theoretical molecular mass, 39 kD) were determined by MALS coupled with gel filtration in the presence of 0.5 mM GDP, and 2.5 mM BeF_3^- with K^+-containing buffers. The estimated molecular masses are shown on the right axis. mAu, milli-Absorbance Unit. The data are representative of at least three repetitions. **(D)** The sizes of OPA1-MGD mutants were determined at 25 µM by AUC in the presence of 0.5 mM GDP and 2.5 mM BeF_3^- with running buffer containing 150 mM KCl and 4 mM $MgCl_2$. Sed, sedimentation. The data are representative of at least three repetitions. **(E)** The GTPase activity of various OPA1-MGD was measured in the presence of 250 mM NaCl or KCl and 4 mM $MgCl_2$. 10 µM of protein was used for each sample. GTP hydrolysis was measured by phosphate release at saturating GTP concentrations (1 mM). Data are presented as the mean ± SD of three measurements and representative of at least three repetitions. **(F)** OPA1-deleted MEF cells were infected with viruses encoding WT or mutant OPA1 as indicated. Mitochondrial morphology was visualized by mitochondrial marker Mito-DsRed and categorized as "fragmented," "filamentous," or "intermediate," examples of which are shown on the left. For each sample, 250 cells were counted. The data are representative of at least three repetitions. Scale bars, 10 µm.

dynamin-1) and a lipid-interacting stalk (equivalent to the PH domain of dynamin-1). At least four OPA1 mutations have sequence similarity to residues in Mgm1-HB2 (Fig. 5 B). N728K (N660 in Mgm1) is at an intermolecular interface between HB2 and the G domain and may contribute to oligomer formation. D603H (K561 in Mgm1) helps stabilize the lipid-interacting stalk on the HB2 domain, whereas L539P (F551 in Mgm1) and V910D (L811 in Mgm1) hold helices in the HB2 domain together.

Finally, we tested key residues newly identified by our structural analysis in OPA1-deleted mouse embryonic fibroblast (MEF) cells. Compared with WT MEFs, knockout (KO) MEFs exhibited fragmented mitochondria (Fig. S3 A) and a loss of cristae structures in the IMM (Fig. S3 B) as reported previously (Del Dotto et al., 2017; Song et al., 2009). When Myc-tagged WT OPA1 was transfected into KO MEFs and Myc signals reached a reasonable intensity, morphological defects were not rescued and became worse in cells expressing more OPA1 (Fig. S3 C). These findings are consistent with overexpression of OPA1 deteriorating mitochondrial health (Cipolat et al., 2004; Olichon et al., 2007b). Nevertheless, a small portion (~20%) of the WT OPA1-expressing cells had a restored mitochondrial shape (Fig. 5 F). Conversely, when OPA1 mutants that were not tested previously, including T407A, D442A, and E444A, were stably expressed (Fig. S3 D), no mitochondrial rescue was detected (Fig. 5 F). When cristae morphology was scored in these cells, similar results were obtained (Fig. S3 E). These results confirm that residues identified in the structure, specifically at the nucleotide-dependent G domain dimer interface, have physiological importance.

Our structural analysis revealed that OPA1-MGD adopts a dynamin-1 GG dimer–like conformation. Both G domains are typically large GTPases and form a nucleotide-dependent dimer. Both the HB1 domain and BSE domain are composed of a relatively short 3-HB intramolecularly linked to the G domain and point in similar directions. The position of HB1 resembles the BSE-semi-closed state in dynamin-1. In previously studied fusogenic DLPs, such as ATL and MFN, the HB closed state was usually termed a post-fusion state, in which the GTP cycle-driven swing of the HB has reached its end. However, in the structure of s-Mgm1 in complex with GDP, HB1 is pointing in the same direction as in GDP- and BeF_3^--loaded OPA1-MGD. In addition, even when HB1 is locked in the closed state, the following HB2 would be predicted to point away, which would not favor the merging of the associating membranes. These results suggest that, even though OPA1 may reorient its HB1 relative to the domain, orienting HB1 would not directly contribute to fusion.

Our biochemical analysis revealed that OPA1 can form nucleotide-dependent and -independent dimers. The combination of these multiple interfaces may lead to higher-order oligomers. The N-terminal coiled coil promotes lipid interaction and subsequent lipid-stimulated GTP hydrolysis. The G domain dimer interface identified here with OPA1-MGD is unique in that all signature G motifs combine forces. It may form transiently or with less frequency, but functional analysis, including lipid-stimulated GTPase assay and cell-based rescue assays, and the occurrence of disease mutations at these sites support this interface playing an essential role. The homotypic interactions identified here would allow the cristae shaping that has been seen with Mgm1. Alternatively, occasional nucleotide-dependent dimerization paces the trimeric assembly that causes fusion, as seen with s-Mgm1.

The structure of OPA1-MGD with GDP and BeF_3^- offers necessary details for understanding the GTP cycle and nucleotide-dependent dimerization of IMM-fusing DLPs. Regardless of the sequence similarity between OPA1 and Mgm1, the G domain of OPA1 differs from Mgm1 in several ways. The α1-β1 loop in OPA1 is much longer than that of Mgm1, whereas the β6-α5 loop is shorter. G319, which lies in the center of Switch 1 and participates in G domain dimerization, is missing in Mgm1. OPA1 also uses unique residues in Switch 1, in addition to previously well characterized ones in all G motifs, to fine-tune its activity. Whether any of these differences explain the higher affinity for GDP and lower GTPase activity of OPA1 remains to be investigated. More importantly, key components for nucleotide-dependent and -independent assembly of OPA1 are not yet reported for Mgm1. Mgm1-MGD and the truncated s-Mgm1 possess nearly identical GTPase activity (Yan et al., 2020), whereas the GTPase activity of s-OPA1 is ~30% higher than that of OPA1-MGD (Fig. 2, C and D). These discrepancies imply that OPA1 functions in yet another manner or differing kinetics than Mgm1.

Materials and methods

Protein preparation

OPA1-MGD was produced from the OPA1-predicted GTPase (263–580) attached to the C terminus (938–960) by an artificial linker (GSGSGSGGS) and cloned into an engineered pET-22b vector with N-terminal 6×His tag. Residues 263–960 of OPA1 were cloned as 263-s-OPA1. For the extended OPA1-MGD and s-OPA1, residues 217–262 were added at the N termini of corresponding constructs. Truncated s-Mgm1 containing residues 184–881 of *S. cerevisiae* Mgm1 and Mgm1-MGD (residues 184–525 and 841–881 connected by an artifical linker of "HGTDSRV") were cloned similarly. The plasmid of OPA1-MGD was transformed

into *E. coli* BL21 (DE3) and the transformed cells cultured at 37°C in Luria-Bertani (LB) media containing 50 mg/liter ampicillin. After reaching an OD 600 of 0.6, the culture was cooled to 16°C and supplemented with 0.2 mM IPTG. After induction at 16°C for 18 h, the cells were harvested and the pellets resuspended in lysis buffer (20 mM Tris-HCl, pH 8.0, 250 or 500 mM NaCl, and 4 mM $MgCl_2$) and then homogenized using an ultra-high-pressure cell disrupter (JNBIO) at 4°C. After centrifugation, the recombinant protein was purified by nickel-nitrilotriacetic acid (Ni-NTA) affinity chromatography and eluted with elution buffer (20 mM Tris-HCl, pH 8.0, 250 mM NaCl, 4 mM $MgCl_2$, and 250 mM imidazole). The protein was then further purified using an HitrapQ column (GE Healthcare). s-Mgm1, Mgm1-MGD, s-OPA1, extended OPA1, and all mutants were purified using the same protocol.

The selenomethionine (SeMet)–substituted protein was expressed in minimal medium that inhibits methionine synthesis. The *E. coli* BL21 (DE3) cells were cultured overnight at 37°C in LB medium containing 50 mg/liter ampicillin, and then transferred into 1 liter of M9 medium supplemented with 50 mg/liter ampicillin and 3% glucose at 37°C until reaching an OD 600 of 0.6. Before induction, 100 mg each of Lys, Phe, and Thr; 50 mg each of Ile, Leu, and Val; and 30 mg SeMet were added to the M9 medium and further incubated for 10 min at 37°C. Next, the culture was cooled to 16°C, supplemented with 0.2 mM IPTG, and allowed to grow at 16°C for an additional 16 h. The SeMet-labeled protein was purified by the same procedure as described for the native protein.

Crystallization, data collection, and structure determination

The crystals of Se-OPA1-MGD/GDP-BeF_3^- were grown at 16°C by mixing 1 µl of protein solution with 1 µl of reservoir solution containing 0.2 M potassium thiocyanate and 20% (wt/vol) polyethylene glycol 3350 (pH 7.0). Crystals appeared after 1 wk and grew to full size within 2 wk. Data were collected to 2.4 Å on a beamline BL17 at Shanghai Synchrotron Radiation Facility and processed and scaled using HKL2000 packages (Otwinowski and Minor, 1997), and Se-OPA1-MGD/GDP-BeF_3^- was determined by molecular replacement using the structure 3T35 in PHENIX (Afonine et al., 2012). The resulting electron density map was displayed with Crystallographic Object-Oriented Toolkit (COOT) and an initial model built manually. Final refinement statistics are summarized in Table 1. Structural figures were drawn using the program PyMOL (http://www.pymol.org/).

ITC

ITC was performed at 16°C with a MicroCal iTC200 instrument (GE Healthcare) as described previously (Yan et al., 2018). Briefly, 2 mM nucleotides in the indicated buffers were injected into 150–200 µM OPA1-MGD. Acquired ITC data were analyzed by the program Origin 7.0 (GE Healthcare) using the "One Set of Binding Sites" fitting model.

MALS

MALS was performed at 25°C with an 18-angle static light scattering detector (DAWN HELEOS II, Wyatt) in conjunction with an analytical size exclusion chromatography column (Superdex200 10/300) as described previously (Yan et al., 2018). For each run, 100 µl of 2 mg/ml purified OPA1-MGD (WT or mutant) was applied after incubating with or without the corresponding ligand (0.5 mM) for 3 h on ice. The column was equilibrated with 20 mM Tris 8.0, 150 mM NaCl/KCl, 4 mM $MgCl_2$, and 2 mM DTT. MALS results were analyzed by the provided ASTRA software.

Analytical ultracentrifugation

For each run, 25 µM OPA1-MGD was used in buffer containing 25 mM Hepes (pH 7.4), 250 mM KCl, and 4 mM $MgCl_2$. Sedimentation velocity experiments were performed at 20°C in a ProteomeLab XL-1 Protein Characterization System (Beckman Coulter), except for 217-MGD at 10°C. All interference data were collected at 42,000 rpm using an An-60 Ti rotor (Beckman Coulter). The AUC data were processed according to a concentration (sedimentation coefficient) distribution model. For sedimentation equilibrium experiments, OPA1-MGD was prepared at three different concentrations (10, 15, and 20 µM). Interference data were collected at three different speeds (12,000, 19,000, and 24,000 rpm) in an An-60 Ti rotor at 10°C and analyzed by SEDPHAT using the monomer–dimer association model.

GTPase activity assay

GTPase assays were performed using the Enzchek phosphate assay kit (Invitrogen). Reactions were performed in a 100 µl volume with 20 µl 5× reaction buffer (1.25M NaCl or KCl, 125 mM Hepes, pH 7.4, and 20 mM $MgCl_2$), 200 µM 2-amino-6-mercapto-7-methylpurine riboside, 0.1 U purine nucleoside phosphorylase, and 10 µM WT or mutant protein as indicated, and incubated for 30 min at 37°C in a 96-well plate (Corning). Reactions were initiated by the addition of 1 mM GTP (Jena Bioscience). The absorbance was measured at 360 nm every 1 min over 1 h at 37°C using a microplate reader (Synergy 4, BioTek). The rate of phosphate release was calculated based on a standard curve.

For membrane-stimulated GTPase activity, 2 µM proteins and 0.2 mM liposomes (Avanti Polar Lipids; 47:23.5:20:8:1.5 mol % POPC/POPE/cardiolipin/soy-PI/Rhodamine-PE) were mixed at room temperature in a buffer containing 25 mM Hepes (pH 7.4), 150 mM KCl, and 4 mM $MgCl_2$ for 30 min. Proteins (1 µM) were then used to measure GTPase activity as mentioned above.

BLI

BLI experiments were performed using the FortéBio Octet96 and streptavidin sensors. Assays were measured in binding buffer (250 mM NaCl, 25 mM Hepes, pH 7.4, 4 mM $MgCl_2$, 0.02% Tween 20) at 30°C. Volumes of 200 µl were used in each well. Biotinylated OPA1 peptides (5 µg/ml) were loaded onto sensors for 90 s, followed by baseline measurements in binding buffer for 60 s. The biosensors were then exposed to different concentrations of OPA1 peptide solution, followed by dissociation in binding buffer. The data were analyzed using software provided by FortéBio (Data Analysis 7.0).

CD

CD experiments were performed on a Biological instrument at 25°C. Peptides (60 µM) were analyzed in 10 mM potassium phosphate (pH 7.5) and 100 mM KCl. Spectra were collected from 190 to 260 nm at a bandwidth of 1 nm and a scan speed of

100 nm/min. Control spectra with buffer were subtracted from the corresponding peptide data.

Flotation assay

The lipids (Avanti Polar Lipids; 47:23.5:20:8:1.5 mol % POPC/POPE/cardiolipin/soy-PI/Rhodamine-PE) were dried to a film, hydrated with 150 mM KCl, 25 mM Hepes (pH 7.4), and 4 mM $MgCl_2$, and extruded through a polycarbonate filter with a pore size of 100 nm. The liposomes (2 mM) were mixed with 2 µM purified protein and incubated at room temperature for 30 min. The 30 µl mixture of proteins and liposomes was mixed with 100 µl of 1.9 M sucrose and overlaid with 100 µl of 1.25 M sucrose and 20 µl of 0.25 M sucrose. The samples were centrifuged in a Beckman TLS 55 rotor at 174,000 *g* at 4°C for 65 min. The gradient was fractionated into five fractions and analyzed by SDS-PAGE and Coomassie blue staining.

Mammalian cell culture, transfection, confocal microscopy, and electron microscopy

OPA1-deleted MEF cells were kindly provided by Z. Song (Wuhan University, Hubei, China) and D. Chan (California Institute of Technology, Pasadena, CA). For mammalian expression, WT or mutant human OPA1 genes were ligated into a pcDNA4/TO vector (transient transfection) or pLenti CMV GFP Puro vector (retroviral transduction). GFP was substituted by OPA1.

OPA1-deleted MEF cells were maintained at 37°C in 5% CO_2. Transfections were performed using Lipofectamine 3000 (Invitrogen) according to the manufacturer's instructions. To generate stable expression cultures, OPA1 KO cells were infected with retrovirus and selected with puromycin. Cells were fixed with 4% paraformaldehyde in PBS for 25 min, permeabilized with 0.1% Triton X-100 for 12 min, and blocked with 3% BSA for 1 h. The cells were then immunostained for 1 h at room temperature with primary antibodies, including mouse anti-Tom20 (BD, 612278, 1:300) or rabbit anti-Myc (abcam, ab9106, 1:400), and then incubated with fluorophore-conjugated secondary antibodies (Alexa Fluor 488–conjugated anti–rabbit or Alexa Fluor 594–conjugated anti–mouse, Invitrogen). All images were captured at room temperature on a confocal microscope (TCS SP5; Leica) with a 63×/1.40 numerical aperture Plan Apochromat oil immersion objective lens using LAS AF version 1.3.1 build 525 software (Leica). For electron microscopy, WT and OPA1 KO MEF cells were fixed with a combination of 4% paraformaldehyde and 2% glutaraldehyde. Images were taken using a FEI spirit 120 kV TEM.

Accession nos.

Coordinates and structure factors have been deposited in the Protein Data Bank under accession no. 6JTG.

Online supplemental material

Fig. S1 shows nucleotide binding and GTP hydrolysis of OPA1. Fig. S2 shows dimerization of OPA1. Fig. S3 shows controls for the mitochondrial morphology rescue assay. Table S1 shows binding affinity of nucleotide to OPA1-MGD measured by ITC.

Acknowledgments

We thank Dr. Alicia M. Prater for proofreading, and the Tsinghua University Branch of China National Center for Protein Sciences (Beijing) for technical support.

J. Hu is supported by the National Natural Science Foundation of China (grant nos. 91854202, 31630020, and 31421002), the Strategic Priority Research Program of the Chinese Academy of Sciences (grant no. XDB39000000) and the Ministry of Science and Technology of the People's Republic of China's National Key Research and Development Program (grant no. 2016YFA0500201) . L. Yan is supported by the National Key Research and Development Program (grant no. 2017YFC0840302) and the National Natural Science Foundation of China (grant no. 20171301816). Z. Rao is supported by the National Key Research and Development Program (grant no. 2017YFC0840300).

The authors declare no competing financial interests.

Author contributions: J. Hu conceived and supervised the project. J. Hu, J. Zhao, Z. Rao, and L. Yan designed the experiments. L. Yan and C. Yu determined the structure with the help of Z. Lou. J. Zhao and C. Yu performed biochemical analysis, and J. Zhao performed all in cell experiments. Y. Qi and X. Guo helped analyze the data. J. Hu wrote the manuscript with input from all authors.

Submitted: 15 July 2019
Revised: 18 February 2020
Accepted: 19 April 2020

References

Afonine, P.V., R.W. Grosse-Kunstleve, N. Echols, J.J. Headd, N.W. Moriarty, M. Mustyakimov, T.C. Terwilliger, A. Urzhumtsev, P.H. Zwart, and P.D. Adams. 2012. Towards automated crystallographic structure refinement with phenix.refine. *Acta Crystallogr. D Biol. Crystallogr.* 68:352–367. https://doi.org/10.1107/S0907444912001308

Alexander, C., M. Votruba, U.E.A. Pesch, D.L. Thiselton, S. Mayer, A. Moore, M. Rodriguez, U. Kellner, B. Leo-Kottler, G. Auburger, et al. 2000. OPA1, encoding a dynamin-related GTPase, is mutated in autosomal dominant optic atrophy linked to chromosome 3q28. *Nat. Genet.* 26:211–215. https://doi.org/10.1038/79944

Ban, T., J.A.W. Heymann, Z. Song, J.E. Hinshaw, and D.C. Chan. 2010. OPA1 disease alleles causing dominant optic atrophy have defects in cardiolipin-stimulated GTP hydrolysis and membrane tubulation. *Hum. Mol. Genet.* 19:2113–2122. https://doi.org/10.1093/hmg/ddq088

Ban, T., T. Ishihara, H. Kohno, S. Saita, A. Ichimura, K. Maenaka, T. Oka, K. Mihara, and N. Ishihara. 2017. Molecular basis of selective mitochondrial fusion by heterotypic action between OPA1 and cardiolipin. *Nat. Cell Biol.* 19:856–863. https://doi.org/10.1038/ncb3560

Belenguer, P., and L. Pellegrini. 2013. The dynamin GTPase OPA1: more than mitochondria? *Biochim. Biophys. Acta.* 1833:176–183. https://doi.org/10.1016/j.bbamcr.2012.08.004

Cao, Y.L., S. Meng, Y. Chen, J.X. Feng, D.D. Gu, B. Yu, Y.J. Li, J.Y. Yang, S. Liao, D.C. Chan, et al. 2017. MFN1 structures reveal nucleotide-triggered dimerization critical for mitochondrial fusion. *Nature.* 542:372–376. https://doi.org/10.1038/nature21077

Carelli, V., M. Sabatelli, R. Carrozzo, T. Rizza, S. Schimpf, B. Wissinger, C. Zanna, M. Rugolo, C. La Morgia, L. Caporali, et al. 2015. 'Behr syndrome' with OPA1 compound heterozygote mutations. *Brain.* • • •:138.

Chappie, J.S., S. Acharya, M. Leonard, S.L. Schmid, and F. Dyda. 2010. G domain dimerization controls dynamin's assembly-stimulated GTPase activity. *Nature.* 465:435–440. https://doi.org/10.1038/nature09032

Chappie, J.S., J.A. Mears, S. Fang, M. Leonard, S.L. Schmid, R.A. Milligan, J.E. Hinshaw, and F. Dyda. 2011. A pseudoatomic model of the dynamin polymer identifies a hydrolysis-dependent powerstroke. *Cell.* 147:209–222. https://doi.org/10.1016/j.cell.2011.09.003

Cipolat, S., O. Martins de Brito, B. Dal Zilio, and L. Scorrano. 2004. OPA1 requires mitofusin 1 to promote mitochondrial fusion. *Proc. Natl. Acad. Sci. USA*. 101:15927–15932. https://doi.org/10.1073/pnas.0407043101

Davies, V.J., A.J. Hollins, M.J. Piechota, W. Yip, J.R. Davies, K.E. White, P.P. Nicols, M.E. Boulton, and M. Votruba. 2007. Opa1 deficiency in a mouse model of autosomal dominant optic atrophy impairs mitochondrial morphology, optic nerve structure and visual function. *Hum. Mol. Genet*. 16:1307–1318. https://doi.org/10.1093/hmg/ddm079

Del Dotto, V., P. Mishra, S. Vidoni, M. Fogazza, A. Maresca, L. Caporali, J.M. McCaffery, M. Cappelletti, E. Baruffini, G. Lenaers, et al. 2017. OPA1 Isoforms in the Hierarchical Organization of Mitochondrial Functions. *Cell Rep*. 19:2557–2571. https://doi.org/10.1016/j.celrep.2017.05.073

Del Dotto, V., M. Fogazza, V. Carelli, M. Rugolo, and C. Zanna. 2018a. Eight human OPA1 isoforms, long and short: What are they for? *Biochim. Biophys. Acta Bioenerg*. 1859:263–269. https://doi.org/10.1016/j.bbabio.2018.01.005

Del Dotto, V., M. Fogazza, F. Musiani, A. Maresca, S.J. Aleo, L. Caporali, C. La Morgia, C. Nolli, T. Lodi, P. Goffrini, et al. 2018b. Deciphering OPA1 mutations pathogenicity by combined analysis of human, mouse and yeast cell models. *Biochim. Biophys. Acta Mol. Basis Dis*. 1864:3496–3514. https://doi.org/10.1016/j.bbadis.2018.08.004

Delettre, C., G. Lenaers, J.M. Griffoin, N. Gigarel, C. Lorenzo, P. Belenguer, L. Pelloquin, J. Grosgeorge, C. Turc-Carel, E. Perret, et al. 2000. Nuclear gene OPA1, encoding a mitochondrial dynamin-related protein, is mutated in dominant optic atrophy. *Nat. Genet*. 26:207–210. https://doi.org/10.1038/79936

Faelber, K., L. Dietrich, J.K. Noel, F. Wollweber, A.K. Pfitzner, A. Muhleip, R. Sanchez, M. Kudryashev, N. Chiaruttini, H. Lilie, et al. 2019. Structure and assembly of the mitochondrial membrane remodelling GTPase Mgm1. *Nature*. 571:429–433. https://doi.org/10.1038/s41586-019-1372-3

Hoppins, S., and J. Nunnari. 2009. The molecular mechanism of mitochondrial fusion. *Biochim. Biophys. Acta*. 1793:20–26. https://doi.org/10.1016/j.bbamcr.2008.07.005

Hu, J., and T.A. Rapoport. 2016. Fusion of the endoplasmic reticulum by membrane-bound GTPases. *Semin. Cell Dev. Biol*. 60:105–111. https://doi.org/10.1016/j.semcdb.2016.06.001

Ishihara, N., Y. Fujita, T. Oka, and K. Mihara. 2006. Regulation of mitochondrial morphology through proteolytic cleavage of OPA1. *EMBO J*. 25:2966–2977. https://doi.org/10.1038/sj.emboj.7601184

Jimah, J.R., and J.E. Hinshaw. 2019. Structural Insights into the Mechanism of Dynamin Superfamily Proteins. *Trends Cell Biol*. 29:257–273. https://doi.org/10.1016/j.tcb.2018.11.003

Kircher, M., D.M. Witten, P. Jain, B.J. O'Roak, G.M. Cooper, and J. Shendure. 2014. A general framework for estimating the relative pathogenicity of human genetic variants. *Nat. Genet*. 46:310–315. https://doi.org/10.1038/ng.2892

MacVicar, T., and T. Langer. 2016. OPA1 processing in cell death and disease - the long and short of it. *J. Cell Sci*. 129:2297–2306. https://doi.org/10.1242/jcs.159186

Meeusen, S., R. DeVay, J. Block, A. Cassidy-Stone, S. Wayson, J.M. McCaffery, and J. Nunnari. 2006. Mitochondrial inner-membrane fusion and crista maintenance requires the dynamin-related GTPase Mgm1. *Cell*. 127:383–395. https://doi.org/10.1016/j.cell.2006.09.021

Olichon, A., G. Elachouri, L. Baricault, C. Delettre, P. Belenguer, and G. Lenaers. 2007a. OPA1 alternate splicing uncouples an evolutionary conserved function in mitochondrial fusion from a vertebrate restricted function in apoptosis. *Cell Death Differ*. 14:682–692. https://doi.org/10.1038/sj.cdd.4402048

Olichon, A., T. Landes, L. Arnauné-Pelloquin, L.J. Emorine, V. Mils, A. Guichet, C. Delettre, C. Hamel, P. Amati-Bonneau, D. Bonneau, et al. 2007b. Effects of OPA1 mutations on mitochondrial morphology and apoptosis: relevance to ADOA pathogenesis. *J. Cell. Physiol*. 211:423–430. https://doi.org/10.1002/jcp.20950

Otwinowski, Z., and W. Minor. 1997. Processing of X-ray diffraction data collected in oscillation mode. *Methods Enzymol*. 276:307–326. https://doi.org/10.1016/S0076-6879(97)76066-X

Qi, Y., L. Yan, C. Yu, X. Guo, X. Zhou, X. Hu, X. Huang, Z. Rao, Z. Lou, and J. Hu. 2016. Structures of human mitofusin 1 provide insight into mitochondrial tethering. *J. Cell Biol*. 215:621–629. https://doi.org/10.1083/jcb.201609019

Rodríguez-Nuevo, A., A. Díaz-Ramos, E. Noguera, F. Díaz-Sáez, X. Duran, J.P. Muñoz, M. Romero, N. Plana, D. Sebastián, C. Tezze, et al. 2018. Mitochondrial DNA and TLR9 drive muscle inflammation upon Opa1 deficiency. *EMBO J*. 37. e96553. https://doi.org/10.15252/embj.201796553

Song, Z., H. Chen, M. Fiket, C. Alexander, and D.C. Chan. 2007. OPA1 processing controls mitochondrial fusion and is regulated by mRNA splicing, membrane potential, and Yme1L. *J. Cell Biol*. 178:749–755. https://doi.org/10.1083/jcb.200704110

Song, Z., M. Ghochani, J.M. McCaffery, T.G. Frey, and D.C. Chan. 2009. Mitofusins and OPA1 mediate sequential steps in mitochondrial membrane fusion. *Mol. Biol. Cell*. 20:3525–3532. https://doi.org/10.1091/mbc.e09-03-0252

Vidoni, S., C. Zanna, M. Rugolo, E. Sarzi, and G. Lenaers. 2013. Why mitochondria must fuse to maintain their genome integrity. *Antioxid. Redox Signal*. 19:379–388. https://doi.org/10.1089/ars.2012.4800

Westermann, B.. 2010. Mitochondrial fusion and fission in cell life and death. *Nat. Rev. Mol. Cell Biol*. 11:872–884. https://doi.org/10.1038/nrm3013

Yan, L., Y. Qi, X. Huang, C. Yu, L. Lan, X. Guo, Z. Rao, J. Hu, and Z. Lou. 2018. Structural basis for GTP hydrolysis and conformational change of MFN1 in mediating membrane fusion. *Nat. Struct. Mol. Biol*. 25:233–243. https://doi.org/10.1038/s41594-018-0034-8

Yan, L., Y. Qi, D. Ricketson, L. Li, K. Subramanian, J. Zhao, C. Yu, L. Wu, R. Sarsam, M. Wong, et al. 2020. Structural analysis of a trimeric assembly of the mitochondrial dynamin-like GTPase Mgm1. *Proc. Natl. Acad. Sci. USA*. 117:4061–4070. https://doi.org/10.1073/pnas.1919116117

Zhang, Z., N. Wakabayashi, J. Wakabayashi, Y. Tamura, W.J. Song, S. Sereda, P. Clerc, B.M. Polster, S.M. Aja, M.V. Pletnikov, et al. 2011. The dynamin-related GTPase Opa1 is required for glucose-stimulated ATP production in pancreatic beta cells. *Mol. Biol. Cell*. 22:2235–2245. https://doi.org/10.1091/mbc.e10-12-0933

JCB

Supplemental material

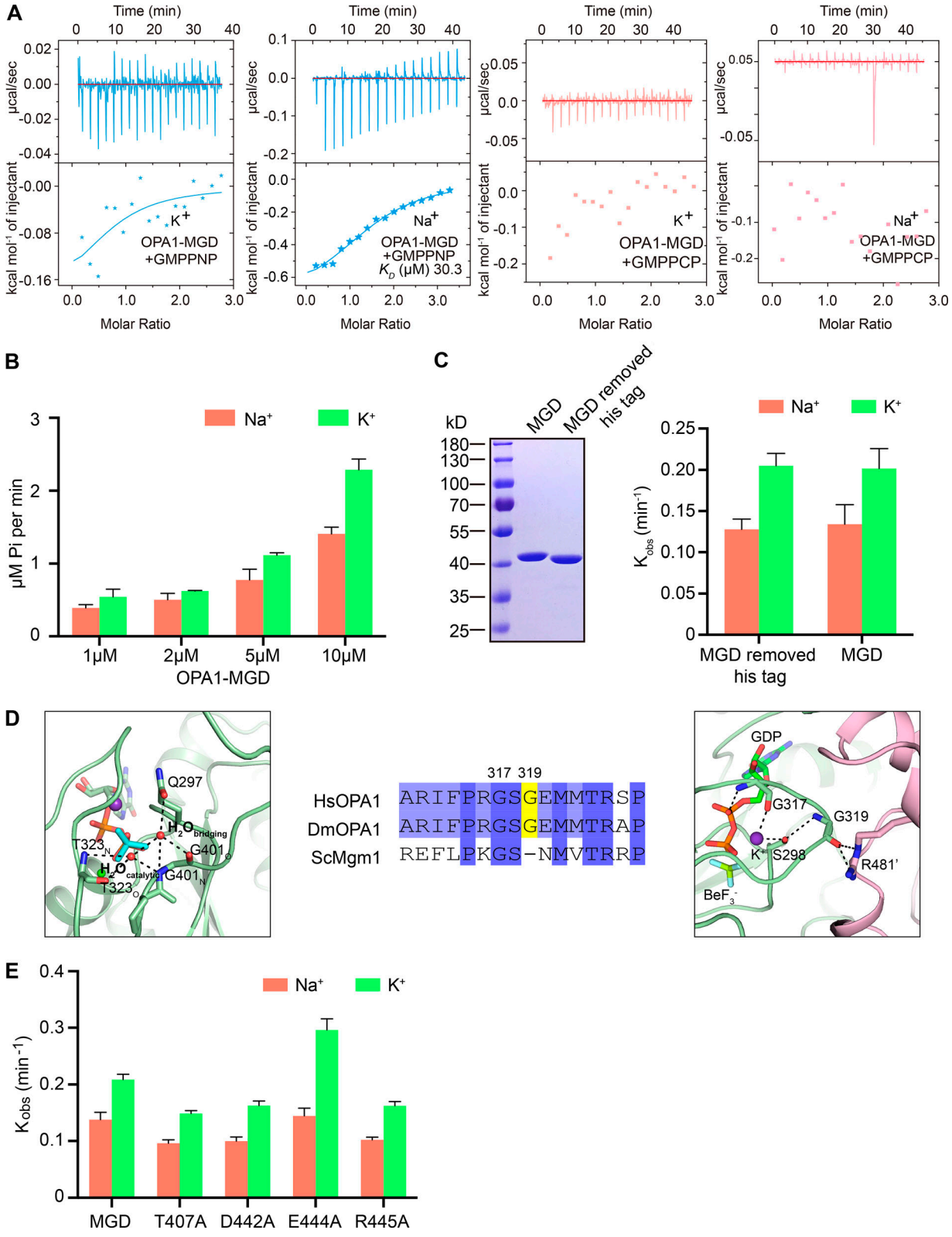

Figure S1. **Nucleotide binding and GTP hydrolysis of OPA1. (A)** Binding affinity of GMPPNP and GMPPCP for WT OPA1-MGD was measured by ITC in the presence of 150 mM KCl or NaCl. 2 mM nucleotides were titrated stepwise into 0.1 mM protein. The K_D, if calculatable, is given in the inset. The data are representative of at least three repetitions. **(B)** GTPase activity of OPA1-MGD was measured in the presence of 250 mM NaCl or KCl and 4 mM $MgCl_2$. The indicated concentrations of OPA1 were used for each sample. GTP hydrolysis was measured by phosphate release at saturating GTP concentrations (1 mM). Data are presented as the mean ± SD of three measurements and representative of at least three repetitions. **(C)** As in B, but with the his-tag removed. **(D)** Sequence comparison of the G2/Switch 1 of OPA1 and Mgm1. Interactions with the catalytic water and bridging water are shown on the left and G319 interactions on the right. **(E)** As in C, but with the indicated OPA1-MGD.

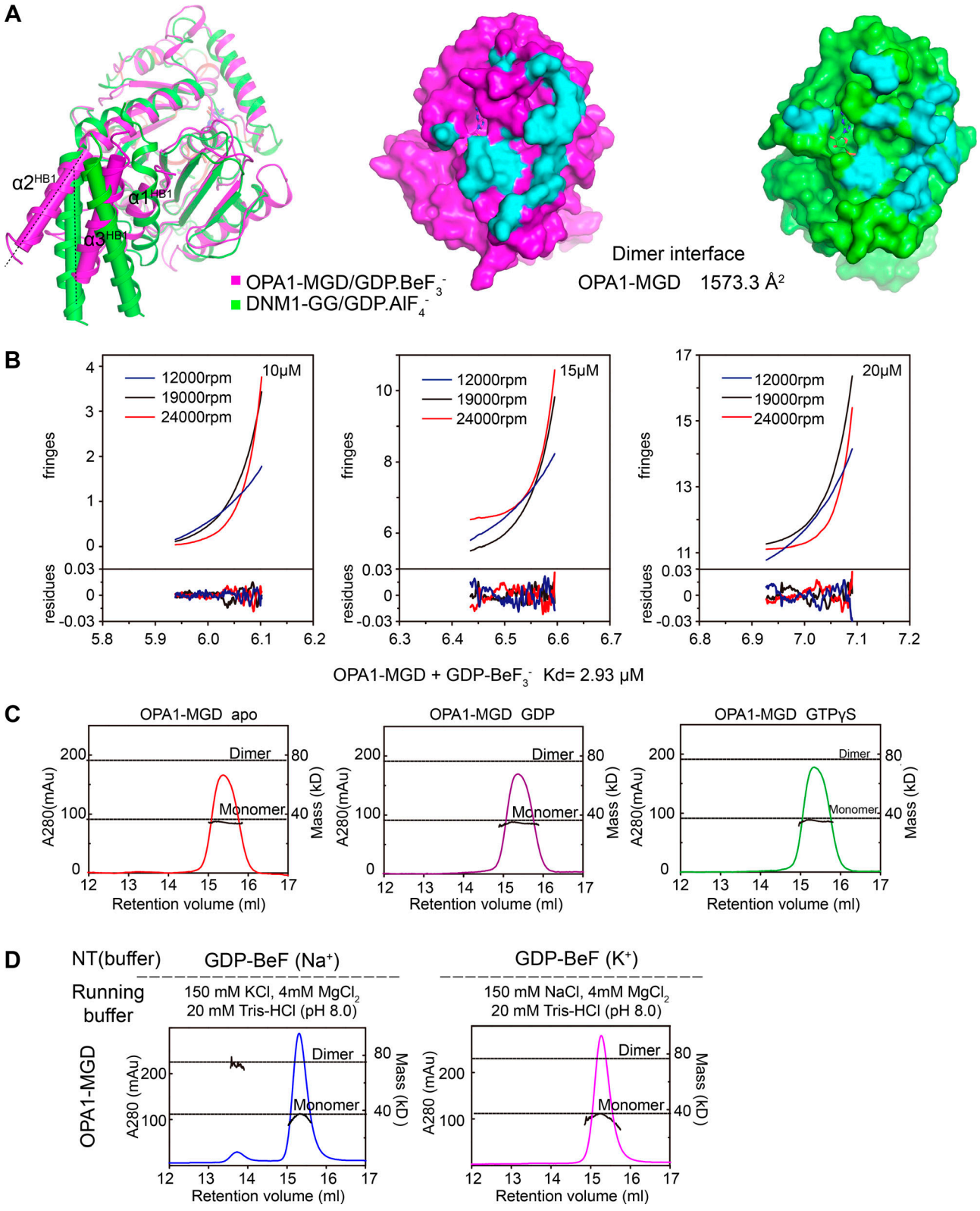

Figure S2. **Dimerization of OPA1. (A)** Superposition of OPA1-MGD and the equivalent region of dynamin-1 (PDB accession no. 2X2F). OPA1 is in magenta, and dynamin is in green. Dimer interfaces are colored in cyan with a comparison of the buried area. **(B)** AUC analysis of WT OPA1-MGD was performed at three concentrations and three different speeds in the presence of GDP-BeF_3^-. The interference profiles at sedimentation equilibrium were used to calculate the K_D (highlighted in green boxes) of the dimers. The corresponding residuals for the fit are shown in the lower portion of each graph. The K_D of the dimer is given. **(C)** OPA1-MGD was incubated with the indicated nucleotides in buffer containing 150 mM KCl. Their sizes were then determined by MALS coupled with gel filtration in the indicated running buffers. The estimated molecular masses are shown on the right axis. The data are representative of at least three repetitions. **(D)** As in C, but with OPA1-MGD incubated with 0.5 mM GDP and 2.5 mM BeF_3^- in a buffer containing 150 mM KCl or NaCl (labeled as K^+ or Na^+).

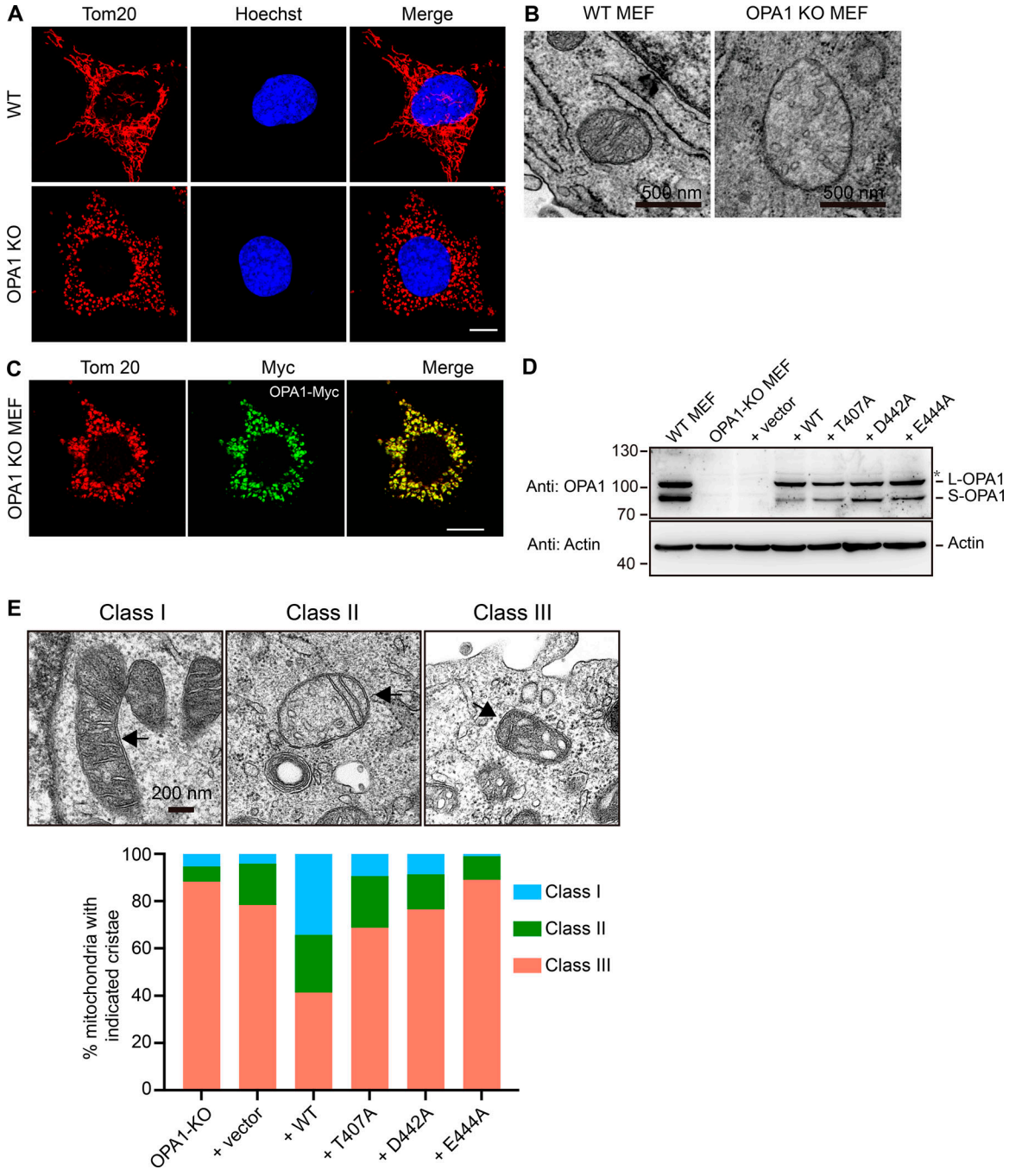

Figure S3. **Mitochondrial morphology rescue assay. (A)** The mitochondrial morphology in WT or OPA1-deleted MEF cells was visualized by indirect immunofluorescence using anti-Tom20 antibodies. The nuclei are stained with Hoechst. Scale bars, 10 µm. **(B)** EM images of WT and OPA1-deleted MEF cells. Representative mitochondria are shown. Scale bars, 0.5 µm. **(C)** Myc-tagged WT OPA1 was transfected into OPA1-deleted MEF cells. Localization was determined using anti-Myc antibodies (green) and compared with mitochondrial marker Tom20 by confocal microscopy. Scale bars, 10 µm. **(D)** Expression of OPA1 used in Fig. 5 F is shown with actin as a loading control. **(E)** EM images of cells used in Fig. 5 F. The cristae morphology is scored as indicated. Scale bar, 0.2 µm.

Table S1 is an Excel table provided online. Table S1 shows the binding affinity of nucleotide to OPA1-MGD measured by ITC.